




Investigation of the adsorption performance of cationic and anionic dyes using hydrocharred waste human hair

Zelal Isik¹ · Mohammed Saleh² · Islem M'barek^{1,3} · Erdal Yabalak⁴ · Nadir Dizge¹ · Balakrishnan Deepanraj^{5,6} 

Received: 22 December 2021 / Revised: 20 February 2022 / Accepted: 10 March 2022 / Published online: 22 March 2022
© The Author(s), under exclusive licence to Springer-Verlag GmbH Germany, part of Springer Nature 2022

Abstract

In this study, waste human hair was converted into hydrochar using the subcritical water medium for the first time. The produced hydrochar from waste human hair (WHH) was employed as an adsorbent for Reactive Red 180 (RR180) and Basic Red 18 (BR18) removal from the aqueous solutions. The adsorption processes were optimized by studying the affecting factors. As a result of the optimization process, the maximum RR180 removal occurred at pH 2, WHH dose of 1 g/L, and at a time of 60 min. For BR18, the best conditions were pH 8, WHH dose of 1 g/L, and time of 60 min. Langmuir and Freundlich models were used to study the adsorptions isotherms. Langmuir isotherm described the RR180 adsorption, while Freundlich had the best fit data for BR18 adsorption. The kinetic studies showed that the adsorptions of RR180 and BR18 were represented by the pseudo-first-order and Elovich models, respectively. Also, the thermodynamic results ensured that the adsorption process occurred spontaneously in nature.

Keywords Human waste hair · Subcritical water medium · Basic Red 18 · Reactive Red 180 · Adsorption

1 Introduction

The anthropogenic pollution of water resources has a detrimental effect on human health [1]. Based on their sources, dyes can be categorized into natural and synthetic. Synthetic dyes can lead to a wide range of problems for the whole ecosystem [2]. Due to the presence of an aromatic ring in their

structures, reactive dyes are destructive pollutants that are toxic and non-degradable [3, 4]. The effects of cationic dyes are also considerable. They have high solubility in water, which blocks the sunlight by reducing the water transparency, causing the death possibility of flora and fauna present in the water bodies [5]. Chong et al. (2014) recognized cationic dyes as carcinogenic matters that do not degrade naturally [6]. It is essential to find innovative, permanent, applicable, environmentalist, and renewable solutions to these hazard alarm bells, which are heard more seriously day by day.

Researchers tried several methods for dyes removal from aqueous solutions. For the biological treatment, several microorganisms were utilized [7–9]. Dotto et al. (2019) examined different coagulants' effects on textile wastewater treatment [10]. Nordin and colleagues (2019) employed a hybrid system of photocatalytic fuel cells and the peroxi-coagulation process in dye degradation [11]. Electrochemical methods [12, 13], membrane bioreactors [14, 15], and adsorption [16, 17] were also employed. Among these methods, the adsorption process has become favored by many researchers. The adsorption process has the advantage of assuring high efficiency with minimal cost and uncomplicated operation [18]. Several adsorbent materials were

✉ Nadir Dizge
ndizge@mersin.edu.tr

✉ Balakrishnan Deepanraj
babudeepan@gmail.com

¹ Department of Environmental Engineering, Mersin University, Mersin 33343, Turkey

² National Agricultural Research Center (NARC), Jenin, Palestine

³ Laboratory for the Application of Materials To the Environment, Water and Energy (LR21ES15), Faculty of Sciences of Gafsa, University of Gafsa, Gafsa, Tunisia

⁴ Faculty of Arts and Science, Department of Chemistry, Mersin University, Mersin 33343, Turkey

⁵ Department of Mechanical Engineering, Jyothi Engineering College, Thrissur 679531, India

⁶ College of Engineering, Prince Mohammad Bin Fahd University, Al Khobar 31952, Saudi Arabia

developed to ensure the beneficial uses of the adsorption process [19–21].

Biochar is a pyrogenic carbon product obtained from biomass under oxygen-limited conditions, which can be applied for soil remediation, fertility enhancement, etc. [22, 23]. Several traditional methods such as pyrolysis, torrefaction, and gasification have been used to produce biochar from different biomass [18]. Hydrochar has many advantages in terms of physicochemical properties and conversion yield compared to biochar [18]. To obtain SWM conditions, the water should be heated at 373–647 K, and sufficient pressure to be applied to keep the water in that temperature range in liquid form [24–26].

Although human hair has been collected in some hairdressers in recent years and evaluated as a commercially profitable waste when viewed more generally, it is unfortunately considered merely as an ordinary waste, as it is seen as unqualified and useless; therefore, it is found in many municipal wastes [27–29]. However, the evaluations of waste human hair's application are interesting approaches. The waste human hair or carbonaceous material obtained from human hair was used in various fields such as a nutrient source for plant growth, glassy carbon microfiber for electrochemical sensing, electrochemical supercapacitor, and soil amendment source were reported [28, 30, 31]. However, to the best of our knowledge, it is the first scientific paper that reports on the production of hydrochar from waste human hair and its evaluation for dye removal. In this study, waste human hair from local hairdresser was collected and converted into hydrochar in environmentally friendly SWM, and then the produced hydrochar was used as an adsorbent for the removal of cationic dye (basic red 18) and anionic dye (reactive red 180) that threaten human health.

2 Materials and methods

2.1 Materials

Waste human hair (WHH) was collected from local hairdresser salons. N_2 gas, supplied from Linde gas (Turkey), was used to provide SWM. Distilled water was obtained using GFL 2001/4 (Burgwedel, Germany). A homemade stainless-steel reactor was employed in the hydrochar synthesis process [18, 32]. For pH adjustment, sodium hydroxide (NaOH, Sigma-Aldrich, 98%) and hydrochloric acid (HCl, Sigma-Aldrich, 37%) were utilized. Reactive Red 180 (RR180) and Basic Red 18 (BR18) were obtained from DyStar.

2.2 Hydrochar preparation via the SWM

Hydrochar was produced in the subcritical water medium. High temperature (373–647K) and adequate pressure to keep water in liquid form are required to obtain a subcritical water medium [33]. The synthesis process of hydrochar from waste human hair is schematized in Fig. 1. Briefly, waste human hair (WHH) samples were collected from local hairdresser's salons and cleaned from dust by washing several times using distilled water and dried. In total, 40 g of dried WHH was placed in the reactor and covered with distilled water. The applied N_2 gas pressure was increased to 30 bar; to keep water in the liquid form. The reactor specifications were mentioned previously [33, 34]. Briefly, a high-pressure (200–250 bars) and temperature-resistant homemade cylindrical steel reactor with 220 cm³ inner volume was employed in the hydrochar synthesis process. The temperature of the reactor was increased to 453 K and kept for 90 min at a constant temperature. After the

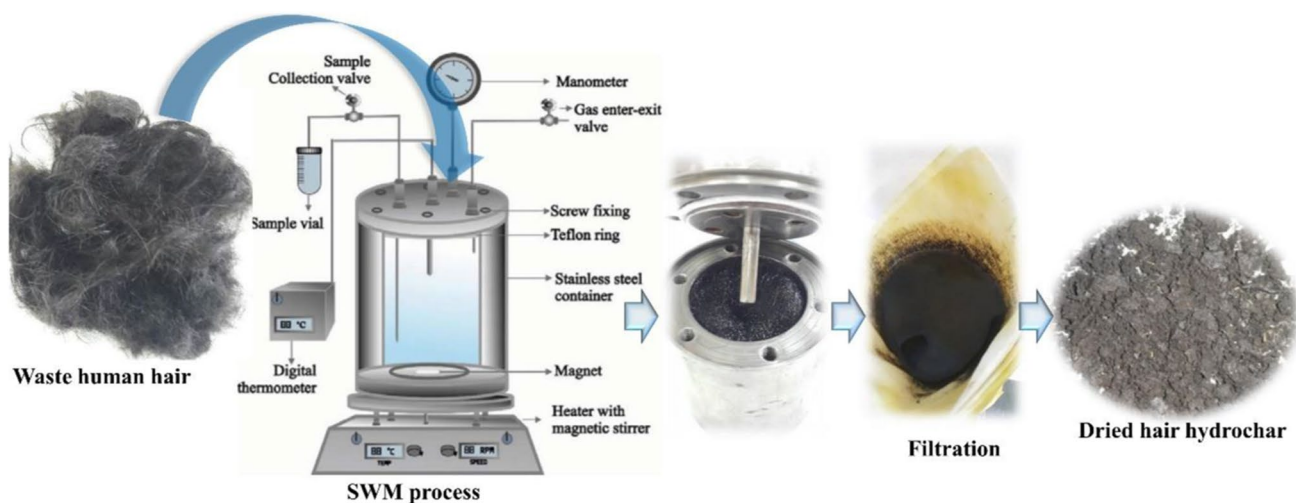


Fig. 1 Hair hydrochar production process in SWM

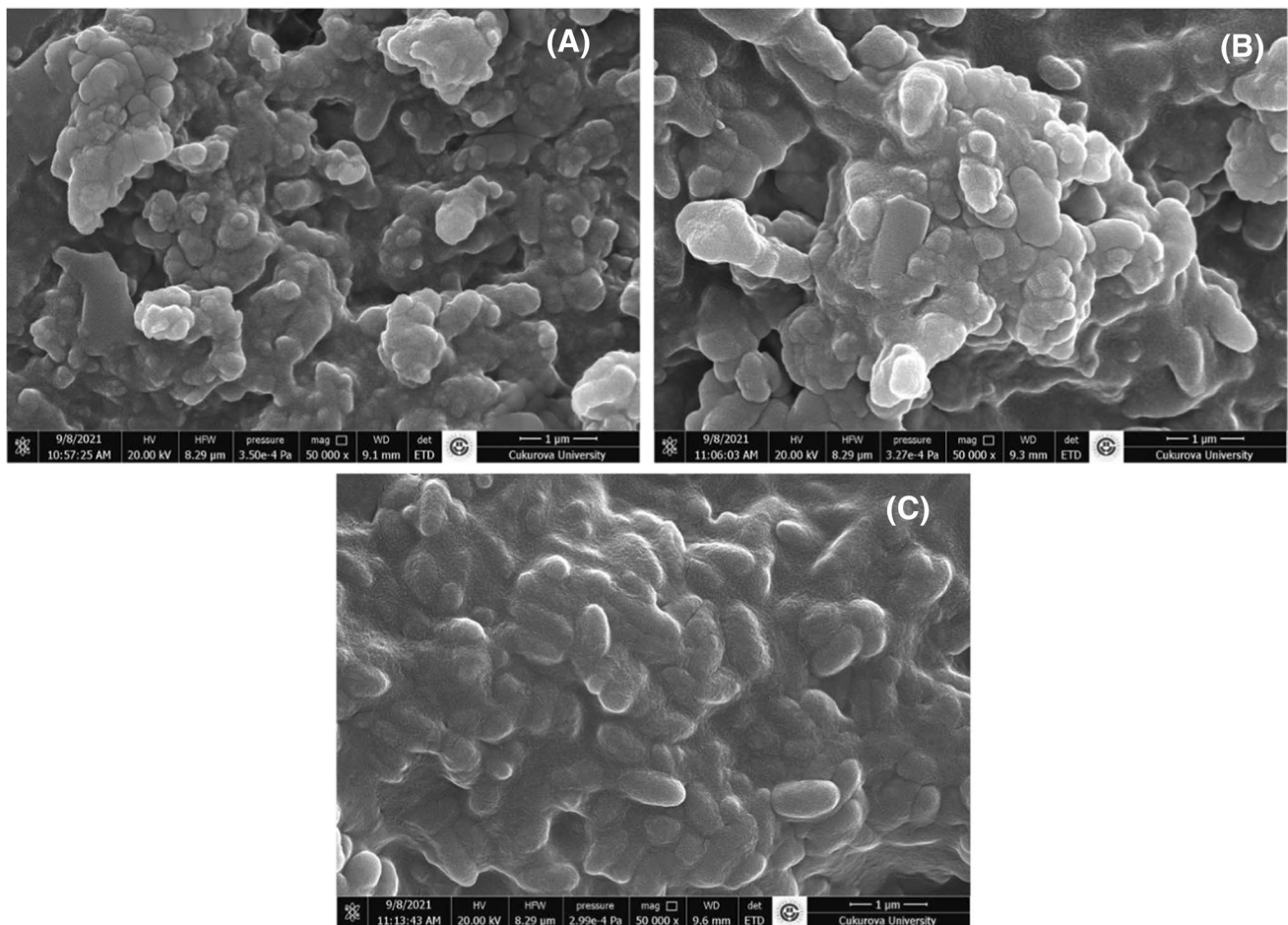


Fig. 2 SEM images of **A** waste hair, **B** BR18 adsorbed waste hair, and **C** RR180 adsorbed waste hair

treatment time, the reactor was cooled to room temperature and the treated sample (hair hydrochar, HH) was filtered and washed three times by deionized water. The HH sample was dried at 371 K and crushed for further application.

2.3 Adsorption of RR18 and BR18 onto HH.

The adsorption experiments of RR180 and BR18 onto HH were carried out by adding the adsorbent into 250-mL Erlenmeyer flasks (ISOLAB) containing 50 mL solutions. The experiments occurred with the aid of an orbital shaker (BIOSAN PSU-20i) that provides agitation of 150 rpm at chamber temperature. A spectrophotometer (HACH DR-3900) was used to measure the changes in concentration at wavelengths of 520 and 486 nm for RR180 and BR18, respectively. Equations 1 and 2 were utilized to obtain the removal efficiencies and adsorption capacities, respectively.

$$\text{Removal efficiency}(\%) = \frac{(C_i - C_e)}{C_i} \times 100\% \quad (1)$$

$$q_e = \frac{(C_i - C_e) \times V}{m} \quad (2)$$

where, C_i and C_e are the initial and the final dyes concentration (mg/L), q_e is the capacity of the adsorption (mg/g), V is the dye solution volume (L), and m is the HH mass (g).

The affecting factors on the adsorption process were studied. The pH effects for the range of 2–10 were studied in the pH optimization experiments. To investigate the pH effects on the RR180 and BR18 removal efficiencies, WHH (1 g/L) was inserted into a 50-mL solution containing 25 mg/L dyes with different pH values (2–10). In same manners, the effects of the adsorbent amount (0.5–2 g/L) and the dyes concentrations (10–50 mg/L) were explored one by one at the optimum pH values. The adsorption was observed at time (5–60 min).

2.4 Adsorption isotherms

Isotherms can be used to describe adsorption by explaining the adsorbent-adsorbate interaction. The experiments of isotherms were done as explained previously [35]. Briefly,

different dye concentrations were exposed to a known amount of HH. Langmuir and Freundlich's isotherms were modeled at the equilibrium points. The non-linear forms of Langmuir [36] and Freundlich's [37] isotherms are shown in Eqs. 3 and 4, respectively.

$$q_e = \frac{Q_{max} \times K_L \times C_e}{1 + K_L \times C_e} \quad (3)$$

Table 1 SEM–EDX analysis of raw HH, RR180 adsorbed HH, and BR18 adsorbed HH

Element	Raw HH (weight %)	RR180 adsorbed HH (weight %)	BR18 adsorbed HH (weight %)
C	45.25	48.82	45.90
N	16.76	16.31	18.26
O	24.30	19.46	22.92
S	13.69	15.41	12.92

$$q_e = K_F \times C_e^{1/n} \quad (4)$$

where, K_L and K_F are Langmuir and Freundlich coefficients, respectively. Q_{max} is the maximum adsorption capacity (mg/g). $1/n$ is the heterogeneity factor.

2.5 Adsorption kinetics

The kinetic models for the removal of RR180 and BR18 onto the prepared HH were studied. The kinetic experiments were conducted by entering known amounts of the adsorbents into 50-mL dye solutions with different concentrations (10, 25, and 50 mg/L). The flasks were agitated and the changes in the concentration over time were tracked until the equilibrium time. The pseudo-first-order model [38], the pseudo-second-order model [39], and the Elovich model [40] were used to describe the adsorption kinetics as shown in Eqs. 5–7, respectively.

$$q_t = q_e(1 - e^{-K_1 t}) \quad (5)$$

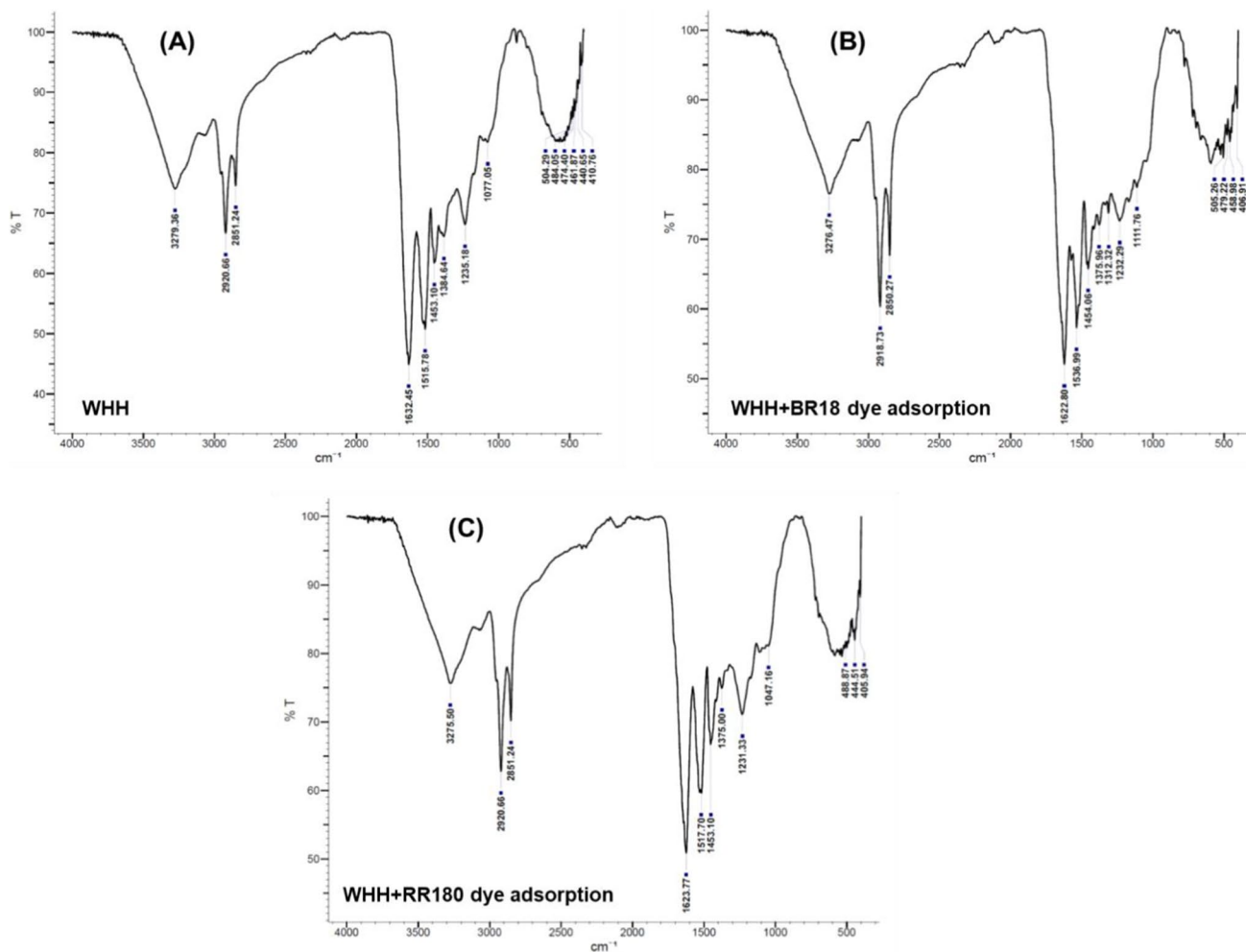


Fig. 3 FTIR spectra of **A** waste hair, **B** BR18 adsorbed waste hair, and **C** RR180 adsorbed waste hair

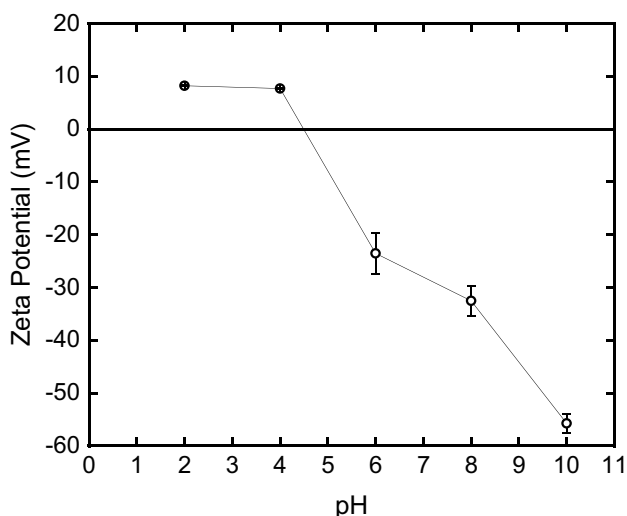


Fig. 4 Zeta potential for the prepared WHH at different pH values

$$q_t = \frac{q_e^2 K_2 t}{1 + q_e K_2 t} \tag{6}$$

$$q_t = \frac{1}{b} \ln(1 + abt) \tag{7}$$

where, q_t is the capacity at time t (mg/g), t is the contact time (min), K_1 is the first order model constant and K_2 is the second order model constant, a is the initial sorption rate (mg/g·min), and b is the desorption constant (g/mg).

The intraparticle diffusion model (IDM) was utilized to identify the diffusion mechanism. IDM can be written as shown in Eq. 8 [41].

$$q_t = K_{IDM} \times t^{1/2} + c \tag{8}$$

where K_{IDM} is the intraparticle diffusion model rate constant (mg/g·min^{1/2}) and c is the boundary layer thickness.

Bangham’s kinetic model was also employed to check whether the pore diffusion is the only mechanism or not. Bangham’s kinetic model equation is presented in Eq. 9 [42].

$$\log\log\left(\frac{C_o}{C_o - q_t m}\right) = \log\left(\frac{K_b m}{2.303V}\right) + \alpha \log(t) \tag{9}$$

where K_b (mL/g/L) and α (< 1) are the Bangham’s model constants, respectively.

2.6 Adsorption thermodynamics

The adsorption thermodynamic is important to judge the feasibility of the adsorption process. In this section, the adsorptions of RR180 and BR18 onto HH were conducted under different temperatures (25, 30, and 35). The other affecting factors were kept constant. At the end of the experiments, the thermodynamic terms were identified with the aid of Eqs. 10–12.

$$\Delta G = -RT \ln K_{eq} \tag{10}$$

$$\Delta G^\circ = \Delta H^\circ - T \Delta S^\circ \tag{11}$$

$$\ln K_{eq} = -\frac{\Delta H}{RT} + \frac{\Delta S}{R} \tag{12}$$

where, ΔG is the change in the Gibbs free energy, R is the universal gas constant (8.314 J/K·mol), T is the absolute temperature (K), K_{eq} is the equilibrium constant, ΔH° is the enthalpy changes (J/mol), and ΔS° is the change in the entropy (J/K·mol).

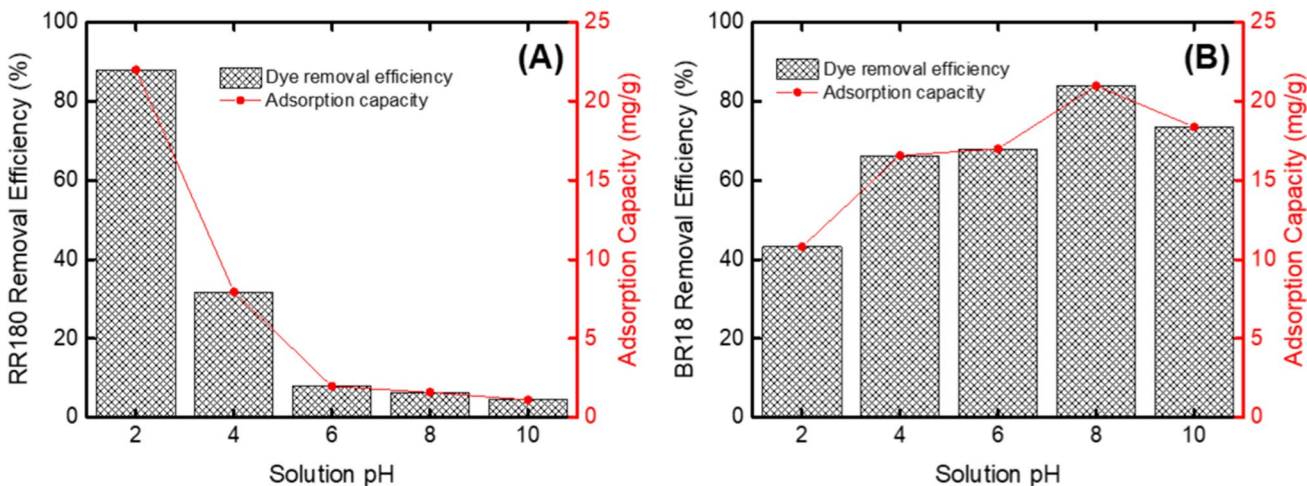


Fig. 5 The variations in the removal efficiency and the adsorption capacity with pH for A RR180 and B BR18

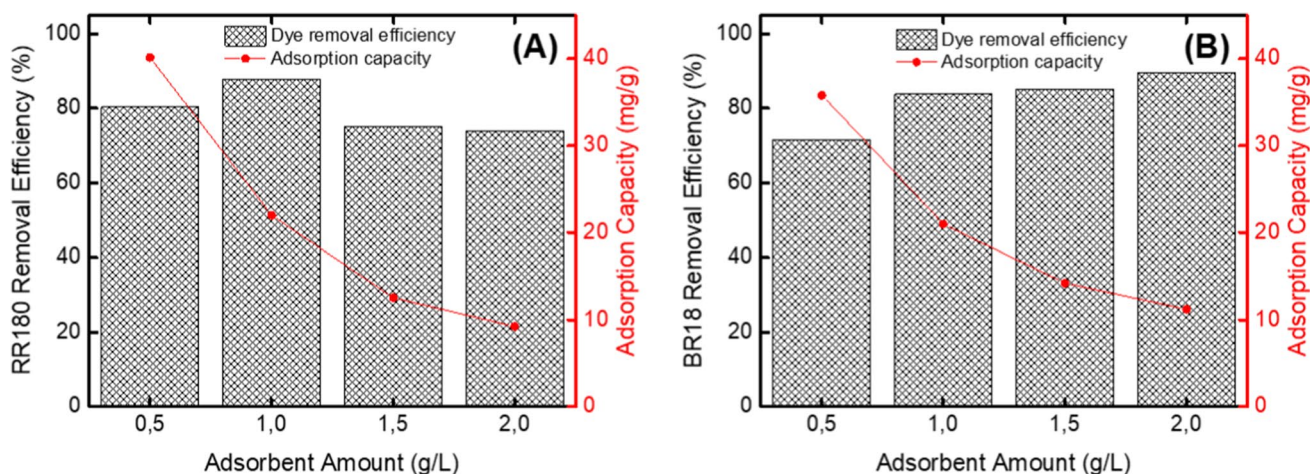


Fig. 6 The removal efficiency and the adsorption capacity variations with the adsorbent dose changes for **A** RR180 and **B** BR18

2.7 Adsorbent characterization

The surface morphology for the prepared hair hydrochar (HH) was scanned using a scanning electron microscopy (SEM, Zeiss Supra 55-Germany). The function groups at the HH surface were recorded using Fourier transform infrared spectroscopy (FT/IR-6700, Jasco) between bands 450 and 4000 cm^{-1} .

3 Results and discussion

3.1 Adsorbent characterization

The surface morphology for the prepared hair hydrochar (HH) was scanned using SEM. The morphology of the raw HH is heterogeneous and consists of the accumulated particles clusters (Fig. 2A). The heterogeneity of the surface increased after the adsorption of BR18 (Fig. 2B) since the dye molecules are amassed randomly on the HH surface, which reduced the spaces between the clusters. In the case of RR180, the clusters were not noticed because the dye molecules filled the pores (Fig. 2C).

The present elements in the HH before and after the adsorption process were determined by Energy Dispersive X-ray Analysis (EDX). The elements in the HH before the adsorption process were carbon (45.25%), nitrogen (16.76%), oxygen (24.3%), and sulfur (13.69%). After the adsorption of RR180, the carbon and sulfur increased to 48.82% and 15.41%, respectively. The increases in those elements confirmed the adsorption of RR180 onto HH since the dye contains carbon and sulfur in the dye structure. In the case of BR18, an increase was noticed in the nitrogen weight

percentage. The nitrogen increased to 18.26% because the BR18 contains 5 nitrogen molecules. This is evidence for the successful adsorption of BR18 onto HH. Table 1 shows the SEM–EDX analysis for the HH before and after adsorption.

FTIR spectrums of waste human hair were obtained before and after dye adsorption (Fig. 3). The peak at 3280 cm^{-1} is related to the N–H stretching mode of proteins. The observed absorptions are the aliphatic C–H stretches of the saturated and unsaturated long-chain fatty acids, alcohols, and esters. The symmetric modes of the methyl (CH_3) and the methylene (CH_2) were recorded at 2921 cm^{-1} and 2850 cm^{-1} , respectively. The functional group C=O stretching coupled with an in-plane bending of the N–H and C–N stretching modes (Amide I band) is noticed at the peak 1632 cm^{-1} , which is broad and strong. The amide II band collected nearby 1516 cm^{-1} is expected to be C=O stretching coupled with C–N stretching and bending deformation of N–H in the protein backbones. The bending deformation of CH_3 vibration of amino acid caused a peak at 1385 cm^{-1} . The contributions of amide III and PO^{2-} asymmetric stretching mode of nucleic acids created an absorption band at 1235 cm^{-1} . In the sulphoxide region at 1073 cm^{-1} , the band corresponding to S–O was observed. The stretching vibrations of the S–S bonds of cysteine are visible in the 505 cm^{-1} regions.

The surface areas and pore-volume for the raw human hair and the WHH were obtained by Brunauer–Emmett–Teller (BET) analysis. The surface area for the human hair was 0.0776 m^2/g , while in the hydrocharred human hair, the surface area reached 3.4107 m^2/g . The pore volume increased from 0.001196 to 0.006321 cm^3/g for raw and hydrocharred hair, respectively.

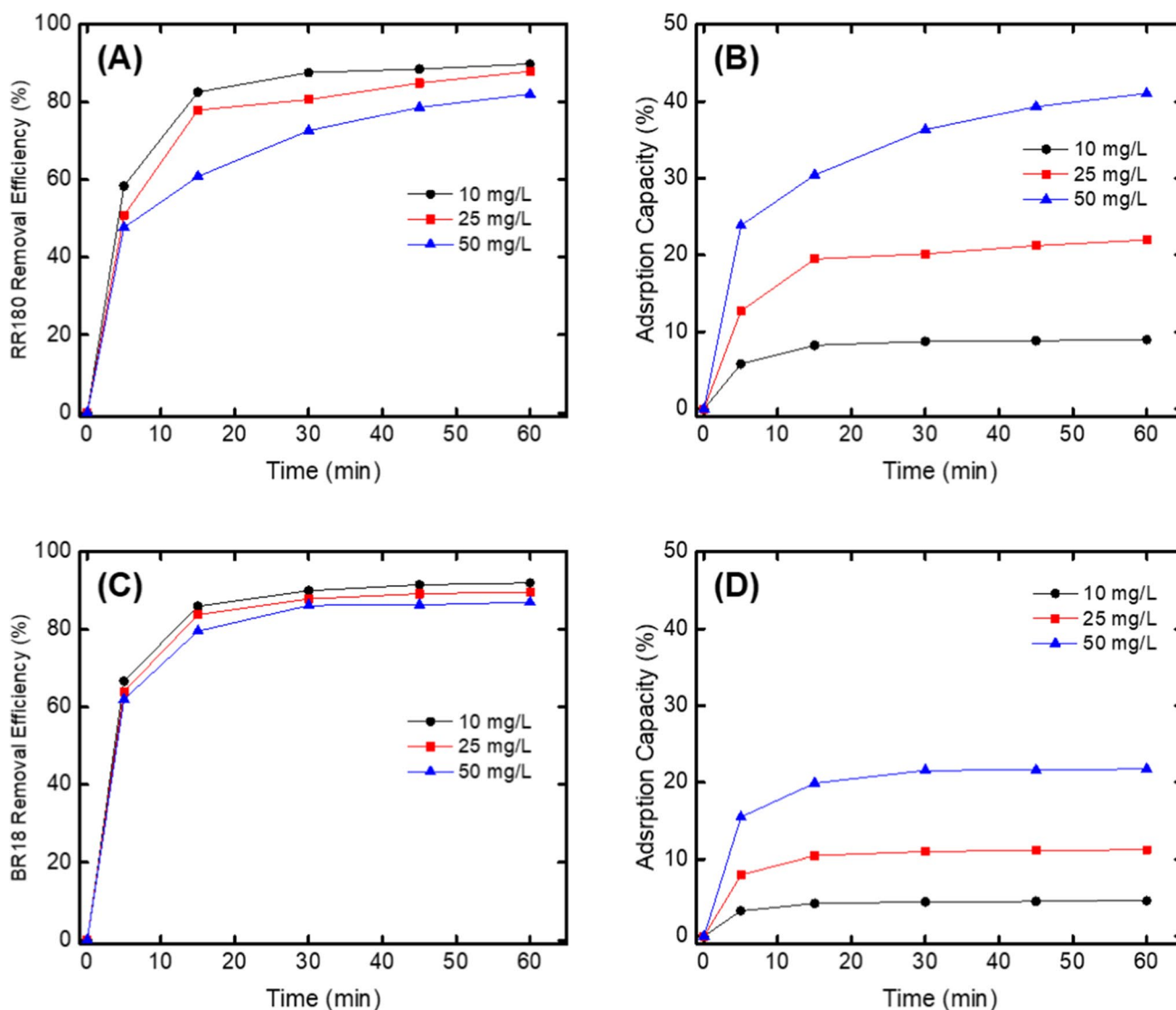


Fig. 7 The effect of the contact time and the initial concentrations factors on **A** the RR180 removal efficiency, **B** the adsorption capacity for RR180, **C** the BR18 removal efficiency, and **D** the adsorption capacity for BR18

3.2 The variations of RR180 and BR180 adsorptions onto WHH with pH

The protonation and deprotonation process at the WHH surface is controlled by pH. The changes of the surface charge for the WHH at distinct pH values were tracked via

Table 2 Isotherms fitting results for RR180 and BR18 adsorption

Isotherm	Parameter	RR180 adsorption	BR18 adsorption
Langmuir	K_L	$0.10431 \pm 1.6262E-4$	$0.10173 \pm 8.14328E-4$
	Q_{max}	84.95204 ± 0.07783	53.71979 ± 0.29614
	R^2	0.9999	0.99719
	Reduced chi-sqr	$6.65748E-5$	0.06603
Freundlich	K_f	9.62665 ± 0.02977	5.52869 ± 0.09789
	$1/n$	0.67377 ± 0.00169	0.73382 ± 0.01044
	R^2	0.99556	0.99977
	Reduced chi-sqr	0.36749	0.01752

a zeta meter (Malvern Zeta Sizer Nano ZS). The results of zeta potential are presented in Fig. 4. According to the zeta analysis results, the WHH had a positive value for the acidic region (2–4). The zero charged point is near a pH value of 4.5. The pH decreased from -23.5 to -55.7 mV when the pH changed from 6 to 10.

The uptake and the capacity variations with the pH variations are shown in Fig. 5. For the adsorption of RR180, the uptake efficiencies and capacities increased with the decreases in the pH values (Fig. 5A). The maximum efficiency (87.92%) and capacity (21.98 mg/g) were obtained at a pH value of 2. The removal efficiency and the adsorption capacity decreased to 4.48% and 1.12 mg/g, respectively at pH 10. RR180 was ionized in water as a polar solvent, which forced the anionic part to move toward the WHH surface. Thus, the removal occurred because of the adsorbent-adsorbate electrostatic interaction. As the pH increased, the hydroxide ions filled the site at the adsorbent surface that causing a reduction in the removal efficiency [43]. Lingeswari and Vimala (2020) obtained a maximum RR180 removal at a pH value of 2 when polyaniline CuCl_2 was utilized as an adsorbent [44]. The possible explanation for the results may be referred to the existence of smaller-sized hydroxide ions that repelled the larger-sized RR180 ions. For the BR18, the increases in the pH raised the removal efficiency from 43.13% at a pH of 2 to 83.92% at a pH value of 8. The adsorption capacity also increased from 10.79 to 20.98 mg/g at pH values of 2 and 8, respectively (Fig. 5B). At higher pH values, the number of the hydroxyl groups raised; thus, the attraction between the cationic dye (BR18) and the negatively

charged sites increased, and the repulsion decreased, which positively affected the adsorption process [45]. Fil et al. (2013) noticed a similar trend for BR18 uptake by the natural Turkish clay [46]. As demonstrated previously [18], the positive charge of the BR18 dye decreases with the increase in the pH values. As the positivity of the solution declines, the attraction force between the negatively charged WHH and the cationic dye decrease, and the removal efficiency falls.

3.3 The effects of the adsorbent dose on RR180 and BR18 adsorption onto WHH

The amount of WHH effects on the removal of the RR180 and BR18 were studied. Various WHH amounts (0.5–2 g/L) were inserted into 25 mg/L dye solution (50 mL volume) and agitated at 150 rpm for 60 min at room temperature. The removal efficiencies for RR180 and BR18 were measured and presented in Fig. 6A and B, respectively. For the RR180 dye, the removal efficiency increased from 80.32% at the adsorbent dose of 0.5 g/L to reach 87.92% at the adsorbent dose of 1 g/L. The increases in the dose beyond 1 g/L reduced the efficiency as the amount of adsorbent increased dye particle was attracted to different adsorbent particles that repulsed each other (same surface charge) into opposite direction that released the adsorbate from the connections [47]. For BR18, the adsorbent amount had a proportional relationship with the removal efficiency. In this study, the most efficient removal rate was obtained at 2 g/L of adsorbent with an efficiency of 89.64%.

Table 3 The kinetic models' results RR180 adsorption onto WHH

Dye Conc. (mg/L)	10	25	50
1st order model			
k_1	0.21221 ± 0.00934	0.1805 ± 0.01513	0.1608 ± 0.03618
q_e	8.82161 ± 0.07248	21.12153 ± 0.35139	38.19265 ± 1.77988
X^2_{Red}	0.0179	0.39503	9.60399
$R^2_{(\text{COD})}$	0.99885	0.9956	0.96725
R^2_{Adj}	0.99856	0.9945	0.95906
2nd order model			
q_e	8.13767 ± 0.65662	19.11865 ± 1.85085	34.18672 ± 4.98576
k_2	$1.31655\text{E}43 \pm 2.06639\text{E}45$	$4.82262\text{E}45 \pm 5.82459\text{E}45$	$3.61716\text{E}45 \pm 4.52934\text{E}45$
X^2_{Red}	1.72462	13.70254	49.71557
$R^2_{(\text{COD})}$	0.88889	0.84746	0.83045
R^2_{Adj}	0.86111	0.80933	0.78806
Elovich model			
a	38.24652 ± 40.20393	33.20184 ± 24.73494	36.26658 ± 5.01598
b	0.80529 ± 0.15045	0.2805 ± 0.04665	0.13911 ± 0.00492
X^2_{Red}	0.20311	1.24309	0.21362
$R^2_{(\text{COD})}$	0.98691	0.98616	0.99927
R^2_{Adj}	0.98364	0.9827	0.99909

Table 4 The kinetic models' results for BR18 adsorption onto WHH

Dye Conc. (mg/L)	10	25	50
1st order model			
k_1	0.26261 ± 0.01504	0.25351 ± 0.01347	0.25051 ± 0.01976
q_e	4.52221 ± 0.04401	11.03172 ± 0.1013	21.37278 ± 0.29312
X^2_{Red}	0.00703	0.03692	0.30813
$R^2_{(COD)}$	0.99827	0.99847	0.99661
R^2_{Adj}	0.99784	0.99809	0.99576
2nd order model			
q_e	4.80938 ± 0.04078	10.36341 ± 1.35199	20.05903 ± 1.21277
k_2	0.09766 ± 0.00727	$-1.91502E45 \pm 4.2547E45$	$2.0905E44 \pm 1.70683E45$
X^2_{Red}	0.00291	1.82788	7.05992
$R^2_{(COD)}$	0.99928	0.92447	0.92231
R^2_{Adj}	0.99911	0.90559	0.90289
Elovich model			
a	102.59489 ± 134.36074	184.34948 ± 238.52333	292.56921 ± 322.94011
b	1.97983 ± 0.34675	0.78106 ± 0.14158	0.39223 ± 0.06262
X^2_{Red}	0.03041	0.20876	0.64077
$R^2_{(COD)}$	0.99252	0.99137	0.99295
R^2_{Adj}	0.99065	0.98922	0.99119

3.4 Contact time and initial concentration effects on the adsorption of RR180 and BR18 onto WHH

The contact time effects on the removals of RR180 and BR18 by WHH were explored. From both dyes, 10, 25, and 50 mg/L solutions concentrations were prepared. For RR180, 1 g/L adsorbent was added to the solutions while 2 g/L were inserted into the BR18 solutions. The changes in the concentrations were tracked over time (5, 15, 30, 45, and 60 min). The removal efficiencies for RR180 at 10, 25, and 50 mg/L were 89.80%, 87.92%, and 82.08%,

respectively (Fig. 7A). Accordingly, the adsorption capacity increased with time and with the increases in the initial concentration. The adsorption capacities for RR180 removal onto WHH were 8.98, 21.98, and 41.04 mg/g at 10, 25, and 50 mg/L, respectively (Fig. 7B). For BR18, 92.0% of the maximum uptake was achieved at an initial concentration of 10 mg/L (Fig. 7C), while the maximum capacity reached 21.76 mg/g at an initial concentration of 50 mg/L (Fig. 7D). Within the first 5 min, all concentrations saw a sharp increase in removal efficiency for both dyes. The increases in the removal efficiencies continued

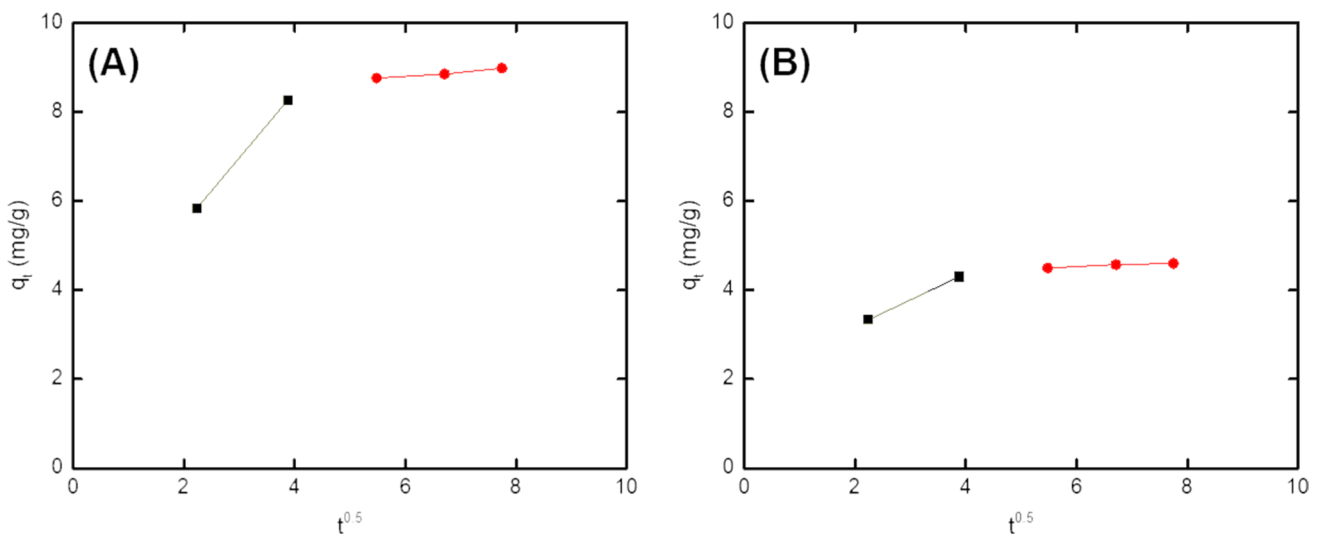


Fig. 8 IDM model for **A** the RR180 removal and **B** the BR18 removal

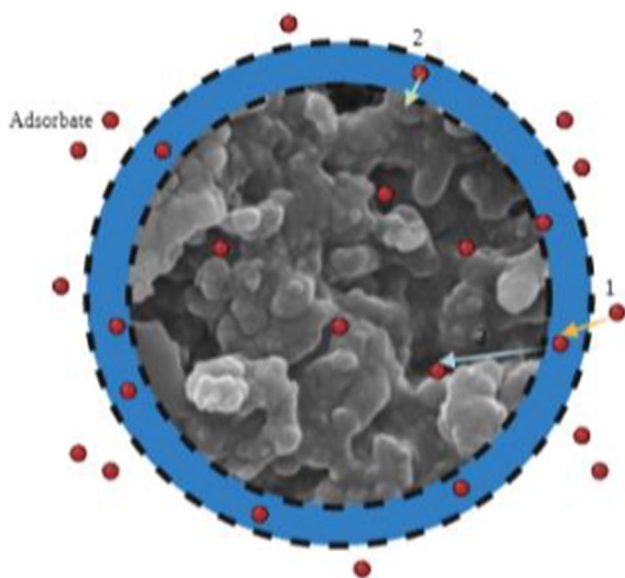


Fig. 9 Adsorption mechanism scheme

with a flatter shape, as shown in Fig. 7. The adsorption capacities also have the same trend. As previously discussed [18, 47], at an earlier stage of the adsorption process, the active sites on the WHH surface caught the dye. A steady-state was achieved as the active sites decreased with time.

3.5 Adsorption isotherms

The non-linear equations for the isotherms presented in Eq. 3 and 4 were fitted with Origin software aid. Many studies demonstrated that non-linear fitting is more accurate than linear fitting [48, 49] since no transformations are required. The fitting results for Langmuir and Freundlich are presented in Table 2. In general, both Isotherms for RR180 and BR18 adsorption have high correlation factors. Since Langmuir isotherm has a higher correlation

factor ($R^2 = 0.9999$) and lower chi-square error values, the removal of RR180 by the WHH can be described by Langmuir isotherm. Based on the Langmuir isotherm, the adsorption of RR180 is assumed to occur in a monolayer with no dye transmigration, and the surface of WHH has a finite active site where the adsorption reaches the saturation point once the sites are pervaded [50, 51]. For BR18, the adsorption can be related to the Freundlich isotherm ($R^2 = 0.99977$), which assumes the formation of heterogeneous multilayers at the end of the adsorption process [52].

3.6 Adsorption kinetics

The kinetic results for RR180 and BR18 adsorptions were fitted to pseudo-first-order, pseudo-second-order, and Elovich models. A comparison of the kinetic parameters and statistical error calculations for RR180 and BR18 adsorption can be found in Table 3 and Table 4. The adsorption of RR180 was found to follow the pseudo-first-order model, while the adsorption of BR18 onto the prepared WHH was found to be represented by the Elovich model because the correlations coefficients are high, and the statistical errors are low. Elovich's model supposes basically that the activation energy grows with the progress in the time of adsorption. Also, the adsorbent surface is energetically heterogeneous.

The solute diffusion onto the adsorbent can be clarified using the intraparticle diffusion model (IDM). The adsorption capacities at any time were plotted against the square root of the time. The IDM graphs for RR180 and BR18 adsorption are presented in Fig. 8.

As presented in Fig. 8, the adsorptions of RR180 and BR18 have three diffusion steps. The first step is a rapid process proposed from the mass transfer of the dyes particles when the adsorbent is added to the solution. The reduction in the uptake speed directs to the film diffusion. Film diffusion is described by the slow motion of the RR18 and

Table 5 The Bangham model results for RR180 and BR18 adsorption onto WHH

Dye Conc. (mg/L)	10	25	50
RR180			
K_b	24.61633 ± 6.7371	39.986 ± 3.48251	16.59177 ± 0.7816
α	0.2919 ± 0.0858	0.21363 ± 0.02805	0.3997 ± 0.01469
X^2_{Red}	0.34803	0.21387	0.23276
$R^2_{(COD)}$	0.97056	0.99745	0.99921
R^2_{Adj}	0.9632	0.99681	0.99901
BR18			
K_b	16.82166 ± 1.75819	15.96026 ± 1.79336	15.13276 ± 1.55139
α	0.15921 ± 0.03119	0.16407 ± 0.03347	0.16718 ± 0.03048
X^2_{Red}	0.03507	0.24213	0.76569
$R^2_{(COD)}$	0.99138	0.99	0.99157
R^2_{Adj}	0.98922	0.98749	0.98947

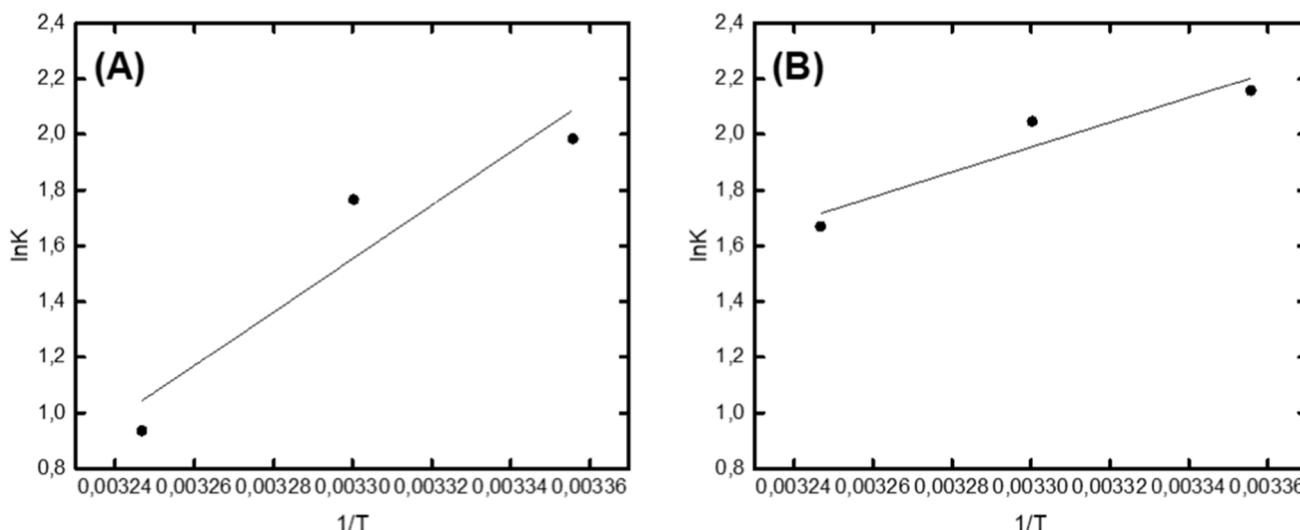


Fig. 10 The relationship between 1/T and ln K for the adsorption of A RR180 and B BR18 onto WHH

Table 6 Thermodynamic results for RR180 adsorption onto the prepared WHH

T (°C)	ΔH (kJ/mol)	ΔS (J/mol.K)	ΔG (kJ/mol)
25	-79.73375	-250.2015	-5.174
30			-3.923
35			-2.672

Table 7 Thermodynamic results for the BR18 adsorption onto the prepared WHH

T (°C)	ΔH (kJ/mol)	ΔS (J/mol.K)	ΔG
25	-37.09873	-106.1781	-5.458
30			-4.927
35			-4.396

BR18 from the boundary layer to the surface of the HH. The movement of the adsorbate to the pores is defined by the third step (Fig. 9).

The multilinearity with no interception through the origin points means that the pore diffusion is not the only rate-controlling step, and film diffusion also takes place in the adsorption of RR18 and BR18. The Bangham model confirms the IDM results, as shown in Table 5. Many researchers noticed a similar mechanism for different types of adsorbents [53, 54].

3.7 Adsorption thermodynamic

Gibb’s free energy, enthalpy, and entropy were identified using the relationships presented in Eqs. 10–12. The adsorption experiments of RR180 and BR18 onto WHH

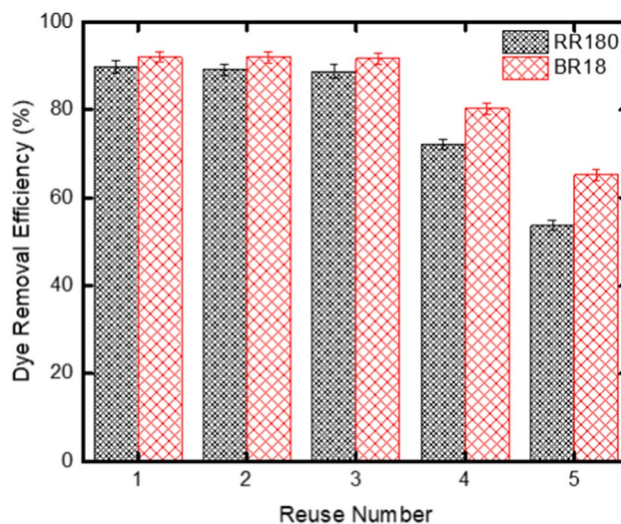


Fig. 11 Reuse cycle of WHH for RR180 and BR18 dye adsorption

were carried out under different temperatures (298, 303, and 308 K). Accordingly, the linear relationship presented in Eq. 12 was plotted as shown in Fig. 10.

The linear relationship between the temperature inverse and the normal logarithm of the equilibrium constant can be used to calculate the enthalpy and the entropy of the adsorption. The enthalpy can be found from the slope of the line, while the line intercept gives the entropy. For RR180, the enthalpy change has a negative sign, which means that the adsorption of RR180 onto WHH is an exothermic process (Table 6). For the same reason, the adsorption of BR18 onto WHH is also exothermic (Table 7). The entropy changes are also negatives for both dyes, which revealed a reduction of

the surface randomness. The Gibbs free energies for RR180 and BR18 adsorption were negative. The negative signs indicate that the adsorption is feasible and spontaneous in nature. As shown by the Gibbs values of RR180 and BR18 (< 20 kJ/mol), the adsorption of the two compounds onto WHH can be considered physisorption.

3.8 Reusability study

Desorption experiments were performed to examine the usability of the adsorbent. At the optimum conditions, desorption experiments were conducted. The HH was used five times for both dyes, at the end of the adsorption, the HH was cleaned with NaOH and washed with distilled water, and used again. According to the results demonstrated in Fig. 11, the efficiency had almost not changed for the first three cycles. At the fifth cycle, the removal efficiencies for the RR180 and BR18 declined to 53.6% and 65.2%, respectively. As a result, the HH adsorbent can be used for three cycles without changes in efficiency.

4 Conclusion

In this study, the human hair waste hydrochar was prepared successfully in SWM for the first time. In the preparation steps, no chemicals were used, and a temperature of 240 °C or less was used in the preparation. The produced hydrochar (WHH) was utilized as an adsorbent for RR180 and BR18. Langmuir isotherm described the RR180 adsorption, while Freundlich had the best fit data for BR18 adsorption. The kinetic studies showed that the adsorptions of RR180 and BR18 were described by pseudo-first-order and Elovich models, respectively. For both dyes, the adsorption process was found to be feasible and naturally spontaneous.

Human hair waste was reported previously as a commercially profitable waste, and this study confirmed that. The use of such wastes can reduce the cost of the adsorbent preparation step. Also, the preparation of WHH adsorbent via the subcritical water medium can be considered as a green process. The prepared hydrochar can be exploited as an effective, low-cost, green adsorbent for RR180 and BR18 dyes removal from the aqueous solution.

Author contribution All authors contributed to the study conception and design.

Material preparation, data collection, and analysis were performed by Zelal Isik, Mohammed Saleh, Islem M'barek, and Erdal Yabalak.

The draft of the manuscript was prepared and finalized by Nadir Dizge and Balakrishnan Deepanraj.

All authors read and approved the final manuscript.

Declarations

Conflict of interest The authors declare no competing interests.

References

- Saleh M, Bilici Z, Kaya M, Yalvac M, Arslan H, Yatmaz HC, Dizge N (2021) The use of basalt powder as a natural heterogeneous catalyst in the Fenton and Photo-Fenton oxidation of cationic dyes. *Adv Powder Technol*
- Thanavel M, Kadam SK, Biradar SP, Govindwar SP, Jeon B, Sadasivam SK (2019) Combined biological and advanced oxidation process for decolorization of textile dyes. *SN Appl Sci* 1(97)
- Ahmed H, Mikhail M, El-Sherbiny S, Nagy K, Emam H (2020) pH responsive intelligent nano-engineer of nanostructures applicable for discoloration of reactive dyes. *J Colloid Interface Sci* 561:147–161
- Tanzifi M, Yaraki MT, Beiramzadeh Z, Saremi LH, Najaffard M, Moradi H, Mansouri M, Karami M, Bazgir H (2020) Carboxymethyl cellulose improved adsorption capacity of polypyrrole/CMC composite nanoparticles for removal of reactive dyes: Experimental optimization and DFT calculation. *Chemosphere* 255:127052
- NN, KR (2020) Selective adsorption and separation of toxic cationic dyes using hierarchically porous SDBS modified vaterite microspheres (Hr-SMV). *J Phys Chem Solids* 146:109598
- Chong KCC, Zakaria S, Sajab M (2014) Vaterite calcium carbonate for the adsorption of Congo red from aqueous solutions. *J Environ Chem Eng* 2:2156–2161
- Pearce C, Christie R, Boothman C, von Canstein H, Guthrie J, Lloyd J (2006) Reactive azo dye reduction by *Shewanella* strain J18 143. *Biotechnol Bioeng* 95(4):692–703
- Elumalai S, Saravanan G (2016) The role of microalgae in textile dye industrial waste Water recycle (phycoremediation). *Int J Pharma Bio Sci*
- Darwesh O, Matter I, Eida M (2019) Development of peroxidase enzyme immobilized magnetic nanoparticles for bioremediation of textile wastewater dye. *J Environ Chem Eng* 7:102805
- Dotto J, Fagundes-Klen M, Veit M, Palácio S, Bergamasco R (2019) Performance of different coagulants in the coagulation/flocculation process of textile wastewater. *J Clean Prod* 208:656–665
- Nordin N, Ho L-N, Ong S-A, Ibrahim A, Lee S-L, Ong Y-P (2019) Elucidating the effects of different photoanode materials on electricity generation and dye degradation in a sustainable hybrid system of photocatalytic fuel cell and peroxi-coagulation process. *Chemosphere* 214:614–622
- Saleh M, Yildirim R, Isik Z, Karagunduz A, Keskinler B, Dizge N (2021) Optimization of the electrochemical oxidation of textile wastewater by graphite electrodes by response surface methodology and artificial neural network. *Water Sci Technol*
- Dos Santos A, Garcia-Segura S, Dosta S, Cano I, Martínez-Huitle C, Brillas E (2019) A ceramic electrode of ZrO₂-Y₂O₃ for the generation of oxidant species in anodic oxidation. Assessment of the treatment of Acid Blue 29 dye in sulfate and chloride media. *Sep Purif Technol* 115747:228
- Berkessa Y, Yan B, Li T, Jegatheesan V, Zhang Y (2020) Treatment of anthraquinone dye textile wastewater using anaerobic dynamic membrane bioreactor: performance and microbial dynamics. *Chemosphere* 238:124539

15. Jegatheesan V, Pramanik B, Chen J, Navaratna D, Chang C, Shu L (2016) Treatment of textile wastewater with membrane bioreactor: a critical review. *Bioresour Technol* 204:202–212
16. Tanzifi M, Yarak MT, Beiramzadeh Z, Saremi LH, Najafifar N, Moradi H, Mansouri M, Karami M, Bazgir H (2020) Carboxymethyl cellulose improved adsorption capacity of polypyrrole/CMC composite nanoparticles for removal of reactive dyes: Experimental optimization and DFT calculation. *Chemosphere* 255:127052
17. Behboudi G, Shayesteh K, Yarak MT, Ebrahimi HA, Moradi S (2021) Optimized synthesis of lignin sulfonate nanoparticles by solvent shifting method and their application for adsorptive removal of dye pollutant. *Chemosphere* 285:131576
18. Saleh M, Bilici Z, Ozay Y, Yabalak E, Yalvac M, Dizge N (2021) Green synthesis of *Quercus coccifera* hydrochar in subcritical water medium and evaluation of its adsorption performance for BR18 dye. *Water Sci Technol*
19. Tan I, Ahmad A, Hameed B (2008) Adsorption of basic dye on high-surface-area activated carbon prepared from coconut husk: equilibrium, kinetic and thermodynamic studies. *J Hazard Mater* 154(1–3):337–346
20. S. Biswas, S. Mohapatra, U. Kumari, B. Meikap and T. Sen (2020) “Batch and continuous closed circuit semi-fluidized bed operation: Removal of MB dye using sugarcane bagasse biochar and alginate composite adsorbents,” *Journal of Environmental Chemical Engineering*, vol. 8, no. 103637.
21. Banerjee S, Dubey S, Gautam R, Chattopadhyaya M, Sharma Y (2019) Adsorption characteristics of alumina nanoparticles for the removal of hazardous dye, Orange G from aqueous solutions. *Arab J Chem* 12(8):5339–5354
22. Zimmerman A, Gao B, Ahn M-Y (2011) Positive and negative carbon mineralization priming effects among a variety of biochar-amended soils. *Soil Biol Biochem* 43:1169–1179
23. Mohan D, Sarswat A, Ok Y, Pittman C (2014) Organic and inorganic contaminants removal from water with biochar, a renewable, low cost and sustainable adsorbent – A critical review. *Bioresour Technol* 160:191–202
24. Yabalak E (2018) Degradation of ticarcillin by subcritical water oxidation method: Application of response surface methodology and artificial neural network modeling. *Journal of Environmental Science and Health, Part A* 53:975–985
25. Yabalak E (2018) An approach to apply eco-friendly subcritical water oxidation method in the mineralization of the antibiotic ampicillin. *J Environ Chem Eng* 6:7132–7137
26. Yabalak E, Külekçi B, Gizir A (2019) Application of ultrasound-assisted and subcritical water oxidation methods in the mineralization of Procion Crimson H-EXL using response surface methodology and artificial neural network. *Journal of Environmental Science and Health, Part A* 54:1412–1422
27. Gupta A (2014) Human Hair “Waste” and Its Utilization: Gaps and Possibilities. *Journal of Waste Management* 2014:1–17
28. Qian W, Sun F, Xu Y, Qiu L, Liu C, Wang S, Yan F (2014) Human hair-derived carbon flakes for electrochemical supercapacitors. *Energy Environ Sci* 7:379–386
29. Saleh M, Yalvac M, Sime F, Mazmanci M (2019) STUDY THE EFFECT OF HAIR STYLE PRODUCTS ON THE QUALITY OF DOMESTIC WASTEWATER- WAX AS CASE STUDY. *Turkish Journal of Engineering* 3(2):97–101
30. Pramanick B, Cadenas L, Kim D-M, Lee W, Shim Y-B, Martinez-Chapa S, Madou M, Hwang H (2016) Human hair-derived hollow carbon microfibers for electrochemical sensing. *Carbon* 107:872–877
31. Zheljzkov V (2005) Assessment of Wool Waste and Hair Waste as Soil Amendment and Nutrient Source. *J Environ Qual* 34:2310–2317
32. Yabalak E, Gizir A (2020) Treatment of Agrochemical Wastewater by Subcritical Water Oxidation Method: Chemical Composition and Ion Analysis of Treated and Untreated Samples. *J Environ Sci Heal A*
33. Yabalak E, Elneccar F (2021) Synthesis of hydrochars in subcritical water medium from solid wastes and investigation of their catalytic effects in the degradation of malachite green using advanced oxidation technique. *Biomass Conv Bioref*
34. Saleh M, Isik Z, Yabalak E, Yalvac M, Dizge N (2021) Green production of hydrochar nut group from waste materials in subcritical water medium and investigation of their adsorption performance for Crystal Violet. *Water Environ Res*
35. Bouras HD, Yeddou AR, Bouras N, Hellel D, Holtz MD, Sabaou N, Chergui A, Nadjemi B (2017) Biosorption of Congo red dye by *Aspergillus carbonarius* M333 and *Penicillium glabrum* Pg1: Kinetics, equilibrium and thermodynamic studies. *J Taiwan Inst Chem Eng* 80:915–923
36. Langmuir I (1918) The adsorption of gases on plane surfaces of glass, mica and platinum. *Am Chem Soc* 40:1361–1403
37. Freundlich H (1906) Over the adsorption in solution. *J Phys Chem* 57:385–470
38. Lagergren S (1898) Zur theorie der sogenannten adsorption gelöster stoffe. *Veternskapsakad Handl* 24(4):1–39
39. Ho Y, Wase D, Forster C (1996) Removal of lead ions from aqueous solution using sphagnum moss peat as adsorbent. *Water SA* 22:219–224
40. Elovich A, Larinov O (1962) Theory of adsorption from solutions of non-electrolytes on solid (I) equation adsorption from solutions and the analysis of its simplest form, (II) verification of the equation of adsorption isotherm from solutions. *Izv Akad Nauk SSSR Otd Khim Naukvol* 2: 209–216
41. Weber W, Morris J (1963) Kinetics of adsorption on carbon from solutions. *J Sanit Eng Div* 89:31–60
42. Tutem E, Apak R, Unal C (1998) Adsorptive removal of chlorophenols from water by bituminous shale. *Water Res* 32:2315–2324
43. Alver E, Metin AÜ (2012) Anionic dye removal from aqueous solutions using modified zeolite: Adsorption kinetics and isotherm studies. *Chem Eng J* 200–202:59–67
44. Lingeswari UD, Vimala T (2020) Adsorption study on removal of reactive blue 21 and reactive red 180 from aqueous medium using polyaniline CuCl₂ in the presence of UV light. *Rasayan J Chem* 13(3):1544–1554
45. Karim A, Mounir B, Hachkar M, Bakasse M, Yaacoubi A (2009) Removal of Basic Red 46 dye from aqueous solution by adsorption onto Moroccan clay. *J Hazard Mater* 168:304–309
46. Fil B, Karcioğlu Karakas Z, Boncukcuğlu R, Yılmaz A (2013) Removal of cationic dye (basic red 18) from aqueous solution using natural Turkish clay. *Glob Nest J* 15(4):529 - 541
47. Isik Z, Saleh M, Dizge N (2021) Adsorption studies of ammonia and phosphate ions onto calcium alginate beads. *Surf Inter* 26:101330
48. Boulinguez B, Le Cloirec P, Wolbert D (2008) Revisiting the Determination of Langmuir Parameters—Application to Tetrahydrothiophene Adsorption onto Activated Carbon. *Langmuir* 24:6420–6424
49. Belhachemi M, Addoun F (2011) Comparative adsorption isotherms and modeling of methylene blue onto activated carbons. *Appl Water Sci* 1:111–117
50. Hameed BH, Din ATM, Ahmad AL (2007) Adsorption of methylene blue onto bamboo-based activated carbon: kinetics and equilibrium studies. *J Hazard Mater* 141(3):819–825

51. Saleh M, Yalvaç M, Arslan H (2019) Optimization of Remazol Brilliant Blue R Adsorption onto *Xanthium Italicum* using the Response Surface Method. *Karbala Int J Mod Sci* 8:1(8)
52. Saleh M, Yalvaç M, Arslan H, Gün M (2019) Malachite Green Dye Removal from Aqueous Solutions Using Invader *Centaurea Solstitialis* Plant and Optimization by Response Surface Method: Kinetic, Isotherm, and Thermodynamic Study. *European Journal of Science and Technology* 17:755–768
53. Inyinbor A, Adekola F, Olatunji G (2016) Kinetics, isotherms and thermodynamic modeling of liquid phase adsorption of Rhodamine B dye onto *Raphia hookerie* fruit epicarp. *Water Resources and Industry* 15:14–27
54. Kajjumba SR, Mahajan R (2016) Equilibrium, kinetics and thermodynamic parameters for adsorptive removal of dye Basic Blue 9 by ground nut shells and *Eichhornia*. *Arab J Chem* 9:S1464–S1477

Publisher's note Springer Nature remains neutral with regard to jurisdictional claims in published maps and institutional affiliations.